

DesignCon 2019

Effect of PCB fabrication variations on interconnect loss, delay, impedance and identified material models for 56 Gbps interconnect designs

Alex Manukovsky, Intel
alex.manukovsky@intel.com

Yuriy Shlepnev, Simberian
shlepnev@simberian.com

Abstract

This paper is the first attempt to separate variations of PCB interconnect geometry and identified material model parameters with the goal to build reliable models for analysis of 56 Gbps PAM-4 links. Test structures were put on the same panels with the production boards. S-parameters for three batches were measured up to 40-70 GHz. To investigate the geometry variations, the structures were cross-sectioned. Variations of impedances, phase delays and losses as well as identified dielectric and conductor roughness model parameters are observed and reported. This is one more step toward the design of predictable PCB interconnects.

Author(s) Biography

Alex Manukovsky is a Technical lead of the Signal & Power Integrity team at Intel Networking Division, responsible for the development of indoor link simulator for high speed serial links, combining both traditional methods of frequency and time domain simulation along with AI machine learning capabilities. Alex focuses on simulation to lab correlation for high speed serial links for PCIe and Ethernet technologies and AI. His past work focused on channel modeling, robust deembedding and calibration techniques for VNA and TDR. His experience includes developing test equipment for compliance testing of serial I/O's as well as lab measurement methodologies for volume testing and Si/Pi simulations. Alex joined Intel in 2010 after receiving his BSc in Electrical Engineering from the Technion – Israel Institute of Technology. He is currently pursuing his Master's degree in System Engineering from the Technion – Israel Institute of Technology.

Yuriy Shlepnev is President and Founder of Simberian Inc., where he develops Simbeor electromagnetic signal integrity software. He received a M.S. degree in radio engineering from Novosibirsk State Technical University in 1983, and the Ph.D. degree in computational electromagnetics from Siberian State University of Telecommunications and Informatics in 1990. He was principal developer of electromagnetic simulator for Eagleware Corporation and the leading developer of electromagnetic software for simulation of signal and power distribution networks at Mentor Graphics. The results of his research are published in multiple papers and conference proceedings.

1. Introduction

Design of predictable PCB interconnects for 56 Gbps PAM-4 links requires analysis to measurement correlation from 1-10 MHz up to 40-50 GHz [1]. There are three necessary conditions to achieve such correlation [2]. First, we need to know the actual PCB interconnect geometry – PCBs are not manufactured as designed. Second, broadband dielectric and conductor roughness models are needed – such models are not available from the material or PCB manufacturers. Third, the accuracy of the analysis software must be systematically validated for this bandwidth. Theoretically, if all three conditions are satisfied, the models should correlate with the measurements. Unfortunately, in reality, it is not possible to know exactly the actual geometry or material properties due to the manufacturing variations [2]. Statistical models are needed, but no data are available from PCB manufacturers to build such models. So far, the only way to build the statistical models is to do it yourself. **To build accurate and reliable models, we need to identify the manufactured transmission line geometries, dielectric and conductor roughness properties as well as assess the manufacturing variation of these quantities.** This paper is the first step in this direction.

To collect the statistical data on manufacturing variations, test structures were put on the same panels with the production boards, measured and cross-sectioned. Variations of geometry and electrical parameters are observed and reported for a large number of samples. Broadband dielectric and conductor roughness models are identified for each sample and variation of the models parameters are observed and reported. **This is the first investigation with an attempt to separate the variations of geometry and electrical properties of materials.** The outcome of this investigation is the data to build statistical models for variations of geometry and for variations of the material model parameters. This is very important step toward design of predictable interconnects for 56 Gbps and beyond. Note that the statistical geometry variations and their effect on the characteristic impedance were investigated by Gary Brist at Intel over 10 years ago [3]. Statistical distribution of losses was investigated at Intel with the standardized SET2DIL methodology [4], with Delta-L and different de-embedding techniques [5]. In this paper we try to separate the geometrical variations from the material model parameters. The results are the statistical distributions for the strip geometry as well as material models suitable for yield or corner-case analysis of 56 Gbps links. **It is not just observation of the geometrical or electrical properties, but is an attempt to build models suitable for design of 56 Gbps links.**

2. Material models to identify

We start with selection of the broadband material models suitable for the analysis of PCB/package interconnects. One broadband model for dielectrics and one broadband model for conductor roughness are selected and described here as the simplest, suitable for PCB characterization, and available in multiple EDA tools.

Wideband Debye (aka Djordjevic-Sarkar or Swensson-Dermer) [6] is the dielectric model that is often used for broadband analysis of PCB and packaging interconnects – it is simple, causal and easy to identify. Expression for complex permittivity of the wideband Debye model can be written as follows:

$$\varepsilon(f) = \varepsilon(\infty) + \frac{\varepsilon_d}{(m2 - m1) \cdot \ln(10)} \cdot \ln \left[\frac{10^{m2} + j \cdot f}{10^{m1} + j \cdot f} \right] \quad (2.1)$$

where f is frequency (note that the original formula of [6] is adjusted here to use linear frequency instead of the radial for convenience). Values of dielectric constant at infinity $\varepsilon(\infty)$ and parameter ε_d can be defined with dielectric constant and loss tangent at just one frequency point (as it is done throughout this paper). Values of $m1$ and $m2$ define position of the first and last pole in the continuous spectrum defined by the model. Those are typically set to very low and very high values outside of the frequency band of interest ($m1=4$, $m2=12$), but they may be also treated as variables in the identification process in cases if dielectric exhibits high dispersion and large growth of the losses for instance. We will use default values for $m1$ and $m2$ and define model (2.1) with only three parameters – dielectric constant (Dk), loss tangent (LT) defined at some frequency (frq). These three numbers uniquely define $\varepsilon(\infty)$ and ε_d in (2.1).

To simulate the effect of conductor roughness, we will use the unified roughness correction coefficient that can be expressed as follows [7]:

$$K_{ri} = 1 + (RF - 1) \cdot F(SR, \delta_s) \quad (2.2)$$

It is applied to the complex transmission line impedance per unit length. In general, it describes multiplicative increase of conductor absorption with frequency as a transition from 1 at lower frequencies (or zero frequency) to maximal value defined by the roughness factor parameter RF . RF can be greater than or equal to 1. Parameter SR is a metric parameter that defines size of a surface model basic element – bump size or ball radius. In general, SR just defines onset frequency of the skin-effect on a rough surface – when SR parameter becomes comparable with skin depth, the losses due to conductor roughness start growing. It may correlate with Ra or Sa parameters measured for a rough surface, but such measurements are usually available only from the copper foil manufacturers. The copper surface is further treated by PCB manufacturer, usually without any numbers to characterise it. Function F describes transition from zero at low frequencies to the unit at high frequencies. Huray-Bracken roughness correction coefficient is used in this paper as the causal version of the Huray snowball correction coefficient with the following transition function [7]:

$$F_{hur}(r, \delta_s) = \left(1 + (1 - j) \frac{\delta_s}{2r} \right)^{-1} \quad (2.3)$$

Where δ_s is skin depth defined as follows:

$$\delta_s = (\pi \cdot f \cdot \mu \cdot \sigma)^{-1/2} \quad (2.4)$$

The first parameter SR in (2.4) is the ball radius from the original Huray model in this case. With the transition function (2.3), the roughness factor in formula (2.2) is related to the original Huray snowball model as follows (see definition of the parameters in [7]):

$$RF = 1 + \frac{3}{2} \frac{N \cdot 4\pi \cdot r^2}{A_{hex}} \quad (2.5)$$

The roughness factor can be also computed from or converted to the Hall-Huray surface ratio (sr) used in some software with the following formulas:

$$RF = 1 + \frac{3}{2} \cdot sr; \quad sr = \frac{2}{3} \cdot (RF - 1) \quad (2.6)$$

3. Material models identification with GMS-parameters

Broadband material model identification up to 40-50 GHz can be done either with generalized modal S-parameters (GMS-parameters) [8], [10] or with the equivalent SPP Light methods [9]. See overview of the other possibilities and comparative analysis in [8] and [9]. Both methods are based on S-parameter measurements for two transmission line segments and technically produce very similar results. We decided to use GMS-parameters as the simplest and the most accurate technique.

GMS-parameters of a transmission line segment are the S-parameters in the modal space normalized to the characteristic impedance of the modes. For the single-ended case GMS-parameters of a transmission line segment with length L are reflection-less by definition and can be written as

$$S_G = \begin{bmatrix} 0 & \exp(-\Gamma \cdot L) \\ \exp(-\Gamma \cdot L) & 0 \end{bmatrix} \quad (3.1)$$

Where Γ or Gamma is the complex propagation constant of the mode $\Gamma = \alpha + j \cdot \beta$, α is attenuation in Np/m, β is phase constant in rad/m. A field solver can be used to build such model. Quasi-static Simbeor SFS solver is used in this paper to extract the modal parameters of strip lines and to compute the GMS-parameters (3.1). On the other hand, if S-parameters are measured for two transmission line segments with length difference L , they can be transformed into GMS-parameters form (3.1) with simple diagonalization of a scattering T-matrix as described in [10]. The diagonalization or “eigenvalue” formulation for the T-matrix of the middle segment was first suggested Soares with co-authors in [11]. Though, the diagonal exponential form of the T-matrix appears as early as 1975 in works of Franzen and Speciale [12] as a part of the de-embedding procedure. The math behind it is simple and magic at the same time. It is based on the fact that T-matrix of a t-line segment is diagonal exponential in the modal space with the normalization to the modal characteristic impedance. If T-matrix of a multiconductor line segment is converted to S-matrix, the result is the GMS-parameters (3.1). The extraction of GMS-parameters can be considered as an incomplete de-embedding – there is no information on the characteristic impedance to re-normalize the matrix to conventional form. Note, that the modal insertion loss and phase delays in

GMS-parameters (3.1) are not "idealized" form of S-parameters. It is exact matrix transformation into 2-diagonal form in case of S-parameters, and into diagonal form in case of scattering T-matrix. The diagonal form of a matrix is the simplest matrix form in the eigenvalue basis - it is not an approximation.

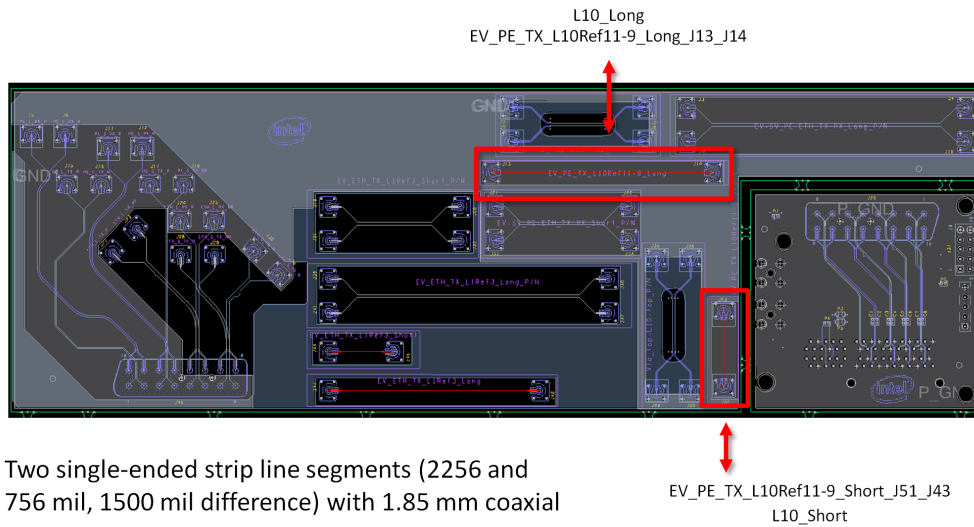
With the measured and modeled GMS-parameters the material model identification procedure adapted to the goals in this paper is as follows:

1. Create strip line segment model with dimensions from cross-sections (or mean values) with dielectric defined as Wideband Debye (2.1) and conductor roughness as Huray-Bracken (2.2 – 2.4) models with preliminary parameters;
2. Identify copper resistivity (RR) by matching measured and computed GMS insertion loss at the lowest frequency (from 10 to 20 MHz);
3. Identify dielectric constant (Dk @ 1 GHz) by matching measured and computed GMS phase delay (from 1 to 40 GHz);
4. Identify loss tangent (LT @ 1 GHz) by matching measured and computed GMS insertion loss at lower frequencies (from 0.05 to 1-2 GHz);
5. Identify conductor roughness model parameters (SR and RF in (2.2)-(2.3)) by matching GMS insertion loss at higher frequencies (from 2 to 25-35 GHz)
6. Adjust dielectric constant (Dk @ 1 GHz) by matching measured and computed GMS phase delay (from 1 to 40 GHz)

It should be done like that, but in reality we had a couple of roadblocks and puzzles that required alteration of the identification algorithm described in the subsequent sections of this paper. Because of the large number of cases to process, the model identification algorithm was scripted and automated with Simbeor SDK. It facilitated the experiments with data from a hundred of measurements and the different model identification scenarios.

4. Test coupon design

The investigation started from the design of coupons suitable for both impedance and material properties investigation. The simplest way to do it is to use the two transmission line segments approach. Two segments can be effectively used to extract GMS-parameters [8] as well as the complex propagation constant or Gamma from measured S-parameters for SPP Light technique [9]. Test coupon design is shown in Fig. 4.1. It contains multiple single-ended and differential strip and embedded microstrip segments. Short and long segments of each line type with length difference 1.5 inch are placed on the coupon. Though, only single-ended strip transmission line segments are used in this paper. We plan to proceed with the microstrip and differential structures as soon as the model building methodology is established with the results obtained with the strip lines (the simplest case). All segments are equipped with snap-on connectors suitable for measurements up to 67 GHz. Micro-probe launches were used on one structure for verification purpose.



Two single-ended strip line segments (2256 and 756 mil, 1500 mil difference) with 1.85 mm coaxial connectors

Fig. 4.1 Test coupon design – only single-ended strip line segments highlighted by red boxes are used in this investigation.

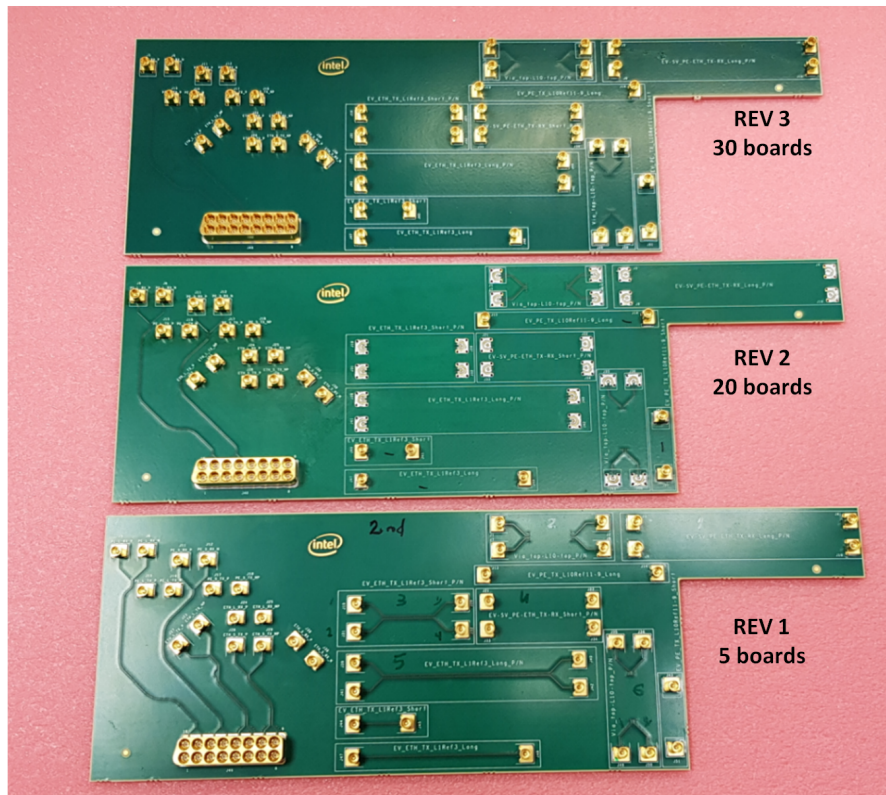


Fig. 4.2. Sample boards from 3 batches. Investigated strip line segments are equipped with snap-on connectors.

Three batches of the same board were manufactured with some modifications of the launches. Samples of the manufactured boards from 3 batches are shown in Fig. 4.2. 5 boards were manufactured in the first batch (Rev1), 20 boards in the second batch (Rev2) and 30 in the third batch (Rev3).

5. Measurement equipment and setup

The goal of this investigation is to measure S-parameters from about 1 MHz up to 50-70 GHz with properties suitable for accurate TDR computations and for GMS-parameters and Gamma extraction, to identify the dielectric and conductor roughness models. Multiple VNAs were tested. The common problem was the passivity violations in S-parameters at lower frequencies with the electronic calibration [2]. That prevented extraction of the material models with the low frequency data. After exploring all options, Keysight PNA Network Analyzer model N5227A with mechanical 1.85mm 85058B Standard Calibration Kit was selected for all measurements. It allows to measure S-parameters from 10MHz to 67GHz with high quality S-parameters through the whole bandwidth. Two adaptors from the snap-on MMPX connectors to 1.85f and to 2.92m are used for each structure equipped with the snap-on MMPX connectors. The calibration was done up to 1.85 mm connectors. A board with two PNA cables during the measurement is shown in Fig. 5.1. The measurement setup was as follows: number of points: 6700; IF BW: 1k; start frequency: 10MHz; stop frequency: 67 GHz; power: -2dbm; averaging: 0.

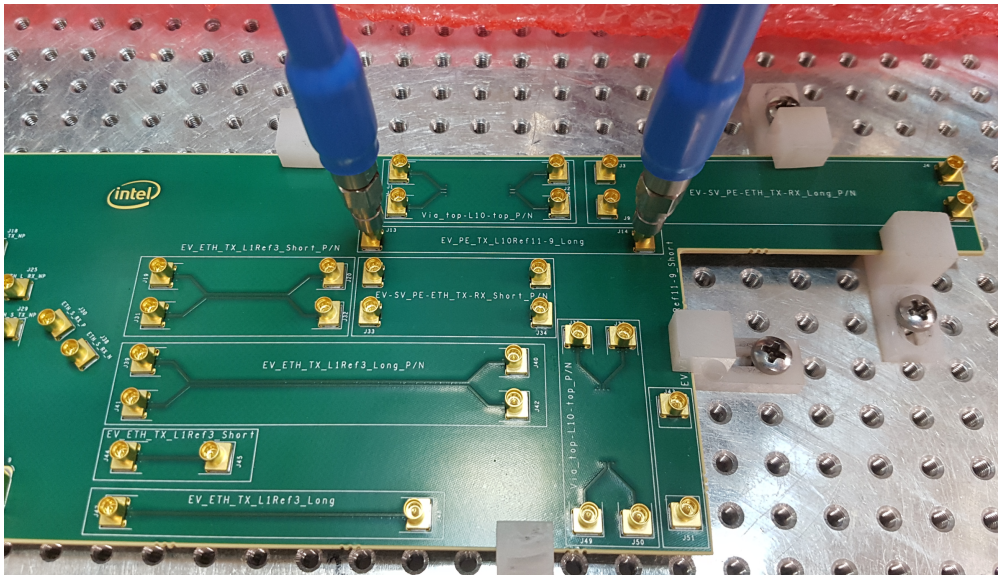


Fig. 5.1. S-parameters measurement setup for long strip line segment.

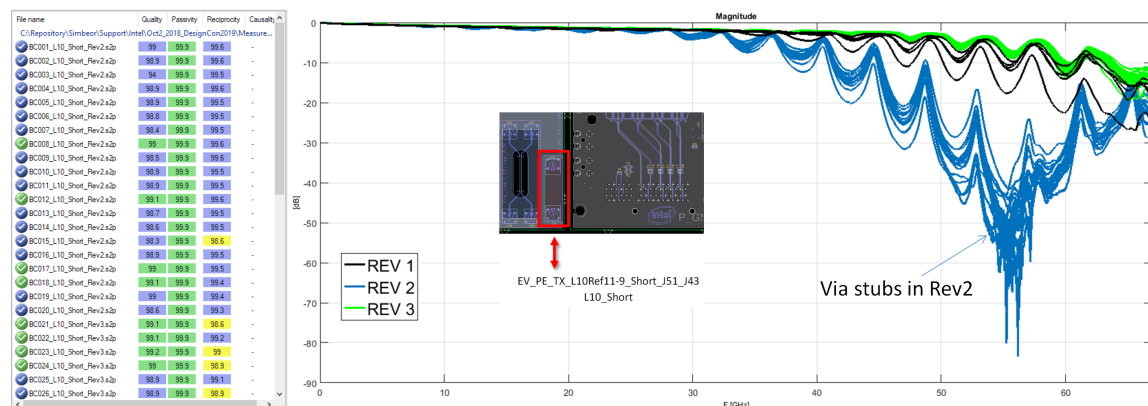


Fig. 5.2. Quality of measured S-parameters (left) and insertion loss for all short strip line segments.

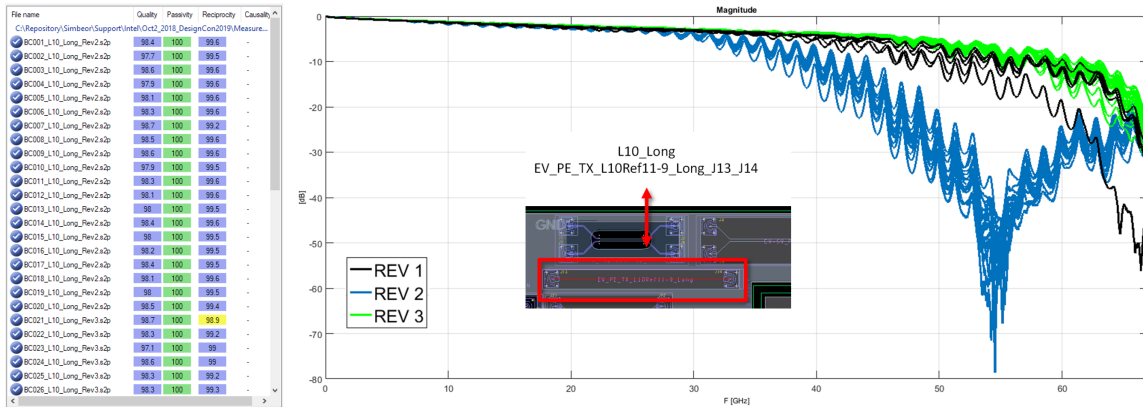


Fig. 5.3. Quality of measured S-parameters (left) and insertion loss for all long strip line segments.

After the measurement technique was defined and validated, S-parameters for 3 batches of the test structures were measured. The results are shown in Fig. 5.2 and 5.3. Quality of the S-parameters was evaluation in Simbeor Touchstone Analyzer with IEEE standardized metrics of passivity, reciprocity and overall quality with the rational approximation (first columns in table of Fig. 5.2 and 5.3). Practically all metrics came out as either good (highlighted in green) or acceptable (highlighted in blue). Structures in Rev2 batch have stubs on the connector launch vias – the stub resonance is visible on the insertion loss plots in Fig. 5.2 and 5.3. It will reduce the bandwidth of the GSM-parameters. The insertion loss in structures of Rev3 was the best - the via-holes at the launch were back-drilled in that batch.

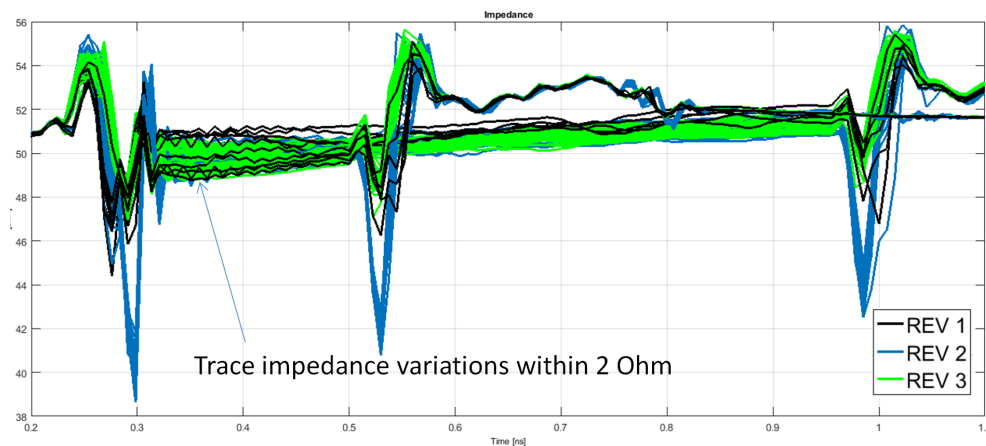


Fig. 5.4. TDR of short and long strip line segments computed with IFFT for all structures.

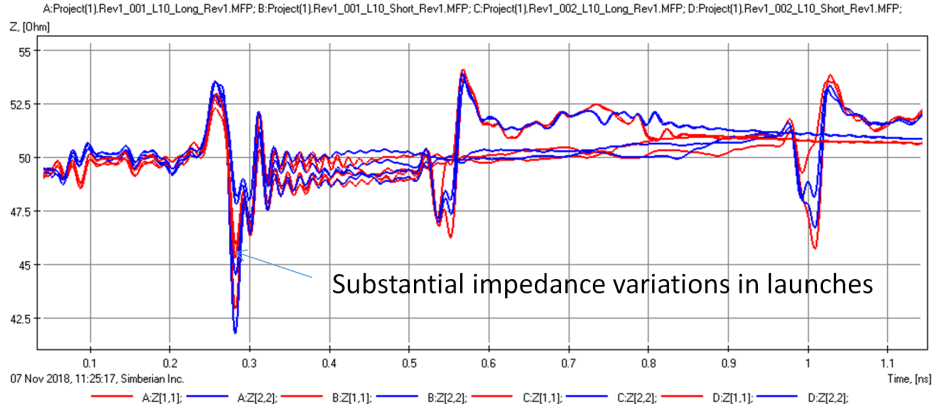


Fig. 5.5. Detailed TDR computed with the rational approximation for structures in Rev1.

TDRs are computed from S-parameters and shown for all structures in Fig. 5.4 and in Fig. 5.5. We observed about 2 Ohm variation in the trace impedances and over 5 Ohm variations in the connectors and launches (or at the boundary between the connectors and launches due to inconsistencies in soldering). That will also restrict the bandwidth of the GMS-parameters. Also, there is about 1 Ohm systematic offset between impedances of the short and long transmission line segments visible in Fig. 5.5. It is possibly due to the orthogonal orientation on the test coupon and difference. As shown in the cross-section chapter, the dielectric fiber was spread only in one direction – that may cause dependency of the impedance from the trace direction, even if the traces are oriented at an angle to the fiber.

At this point we provide just simple observations and pre-qualification of the measured data without any statistical processing of the results. This is because of the insertion loss is the frequency-dependent parameter and includes the effect of the reflections. Considering the characteristic impedance of the strip line, it is frequency-dependent too and cannot be uniquely identified from the TDR. The observed impedance values depend on the stimulus spectrum, depend on the observation time and depend on what is going on before the strips (discontinuities and trend up due to conductor resistance). Thus, all statistical observations here are done with the models matching measured GMS-parameters in the subsequent sections.

6. Extraction of GMS-parameters

As was outlined in section 3, S-parameters of two line segments can be used to extract the reflection-less GMS-parameters (3.1). GMS-parameters of single-ended line segment is a 2x2 symmetric matrix described with just one complex function of frequency characterizing pure insertion loss and delay in a transmission line segment. Magnitude of this function is GMS insertion loss or attenuation and negative angle of the GMS transmission parameter divided by radian frequency is the phase delay in the transmission line segment with 1.5 inch length in this case.

The extracted GMS-parameters are shown in Fig. 6.1 as attenuation and phase delay plots for all investigated structures. The phase delay is smooth and suitable for the material model identification up to 40 GHz for all structures. Technically, it can be extracted even up to 60 GHz for the Rev2 batch, but it is just smooth continuation with slight decrease of the delay with the frequency – not much information. Contrary to that,

the attenuation is noisy – the periodic notches can be observed on all attenuation plots and are particularly bad in batch Rev2 with the via stubs.

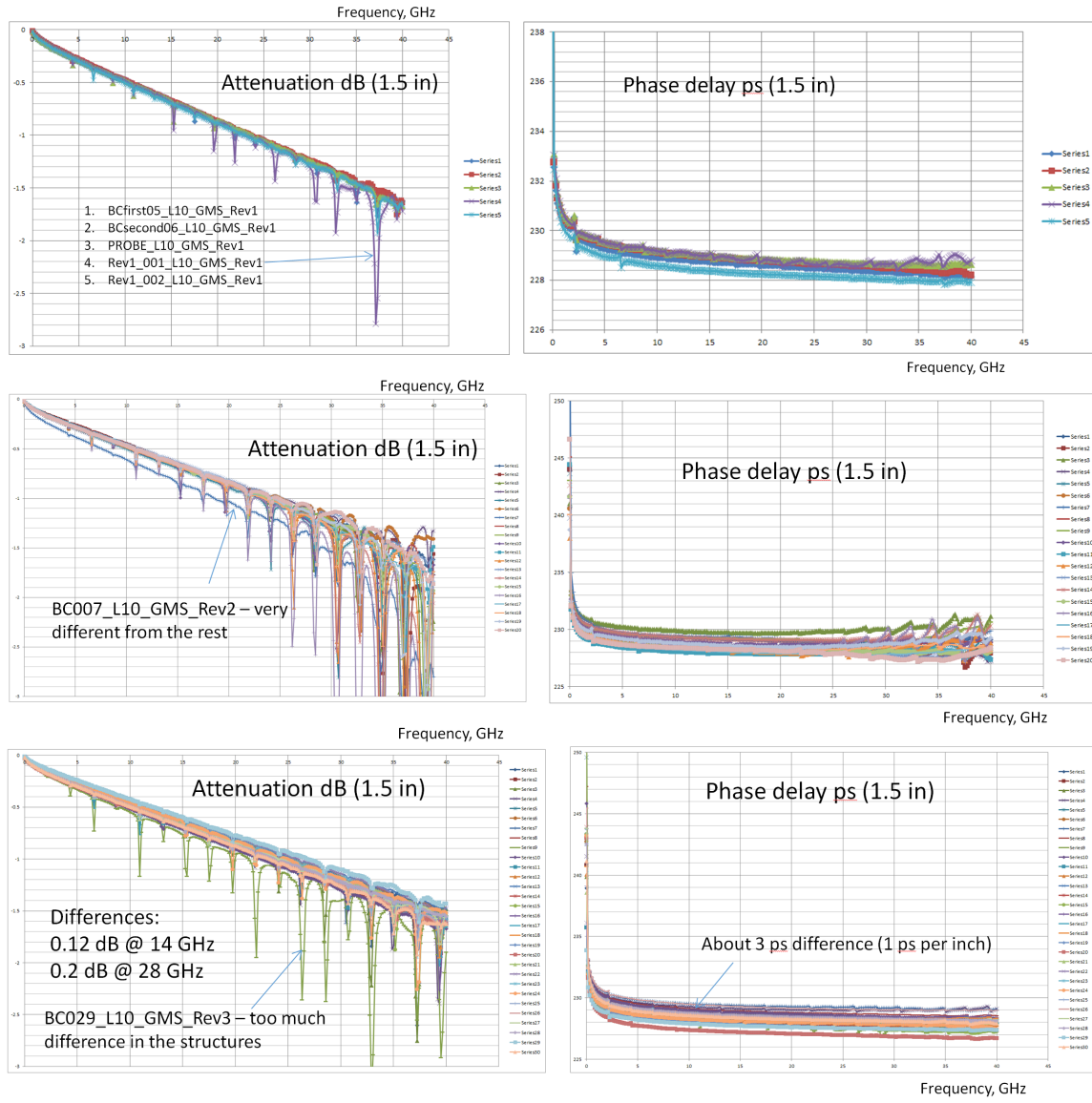


Fig. 6.1. GMS insertion loss or attenuation (left plots) and GMS phase delays extracted of strip line segments measured for batches Rev1 (top graphs), Rev2 (middle graphs) and Rev3 (bottom graphs).

The notches are caused by physical differences in the launches in the short and long segments. The frequency range of the attenuation usable for the material model identification is restricted by that down to 35 GHz for Rev1 and Rev3 batches and to 25 GHz for the Rev2 batch. Though, this is not a problem, because of the use of the analytically defined material models and use of the transmission line models. The notches can be removed with the post-processing of the attenuation. Alternatively, the frequency sampling can be adjusted in the models for the identification to avoid the periodic peaks as it is done in the next section. We expect that the models identified with the GMS-parameters with the reduced bandwidth will be usable up to 50 GHz. Considering the overall variations, we can observe relatively large variations in the GMS insertion loss

and phase delay as shown at the bottom plots in Fig. 6.1. The question is what causes the loss and phase delay variations? Is it geometry or material properties? We will try to answer this.

7. Cross-sectioning and geometry variations

To find out the reason for the impedance, losses and phase delay variations, all measured test structures were cross-sectioned and geometry variations are observed. Both short and long segments were cross-sectioned, but measurements from the short segments are used for the material model identification.

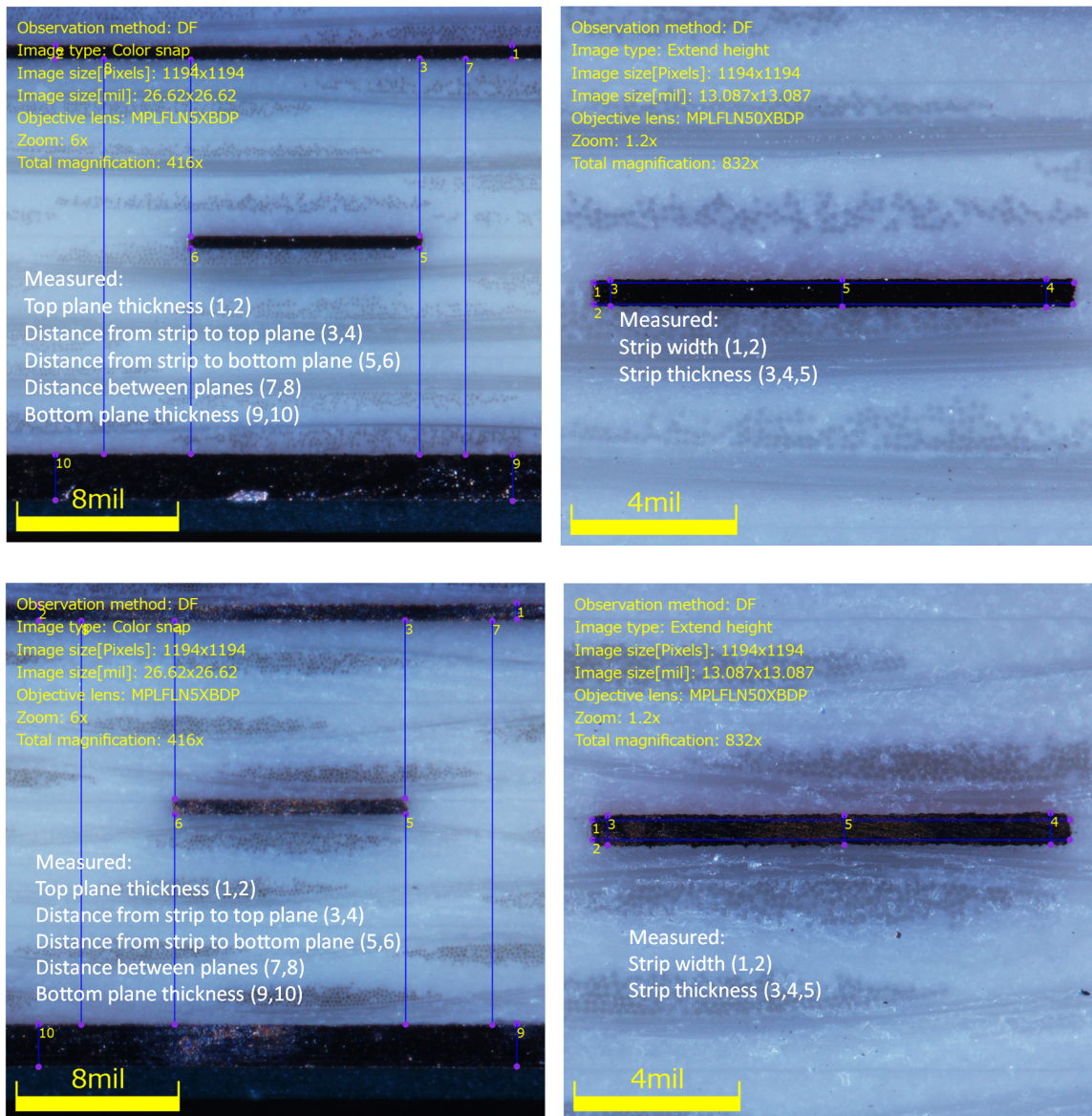


Fig. 7.1. Cross-section views for short line segment (top) and for long line segment (bottom).

All measurements are taken at 2 or 3 locations as illustrated in Fig. 7.1 and average values are plotted in Fig. 7.2 – 7.3 for each board in 3 batches. The major contributor to the conductor losses at lower frequencies and impedance variations is the cross-section of the trace. As we can see from the data on Fig. 7.2 the cross-section of the trace can be different from sample to sample by as much as 30%! Most of the variations are in the thickness of the trace. It is caused by variations in the foil thickness or, more likely, by foil processing by PCB manufacturer [3]. If such variations take place along the traces, that can contribute to the impedance variations along the segments and the losses variations observed at lower frequencies. It also introduces uncertainties into the identification process. To confirm that, we have to cut the same strip line segment at multiple locations along the trace.

Considering the thickness of the laminate above and below the strip, the variations are not so large as shown in Fig. 7.3. The dielectric thickness affects mostly the characteristic impedance and not the losses. The material parameters will be not very sensitive to the variations of these parameters. Again, we observe only board to board variations – the same variations may take place along the traces that may also contribute to the impedance variations along the strip segments.

From Fig. 7.1 we can also observe some differences in spreading of the fiber bundles. The fiber bundles across the short line cross-section look wider than across the long line cross-section. The traces were routed at a small angle to the fiber, but long and short segments are routed at 90 degrees. That difference can explain systematic offset in the impedance observed earlier on TDR plots (see Fig. 5.5).

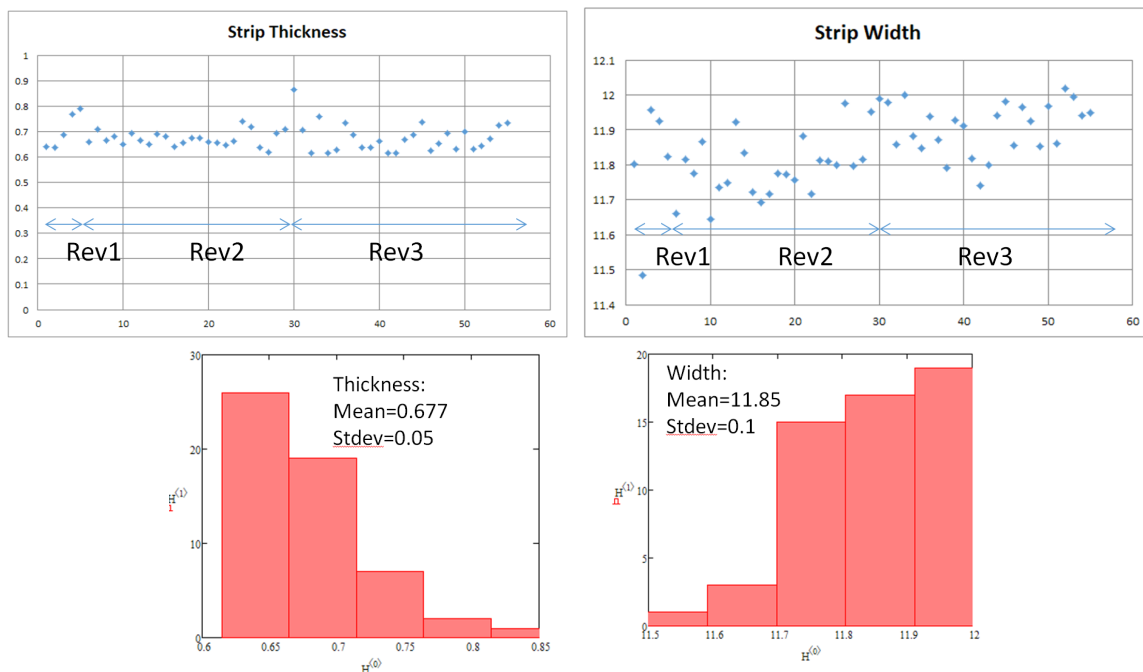


Fig. 7.2. Strip thickness (top left graph) and width (top right graph) measured from cross-sections of all short strip line segments and corresponding histograms (bottom plots).

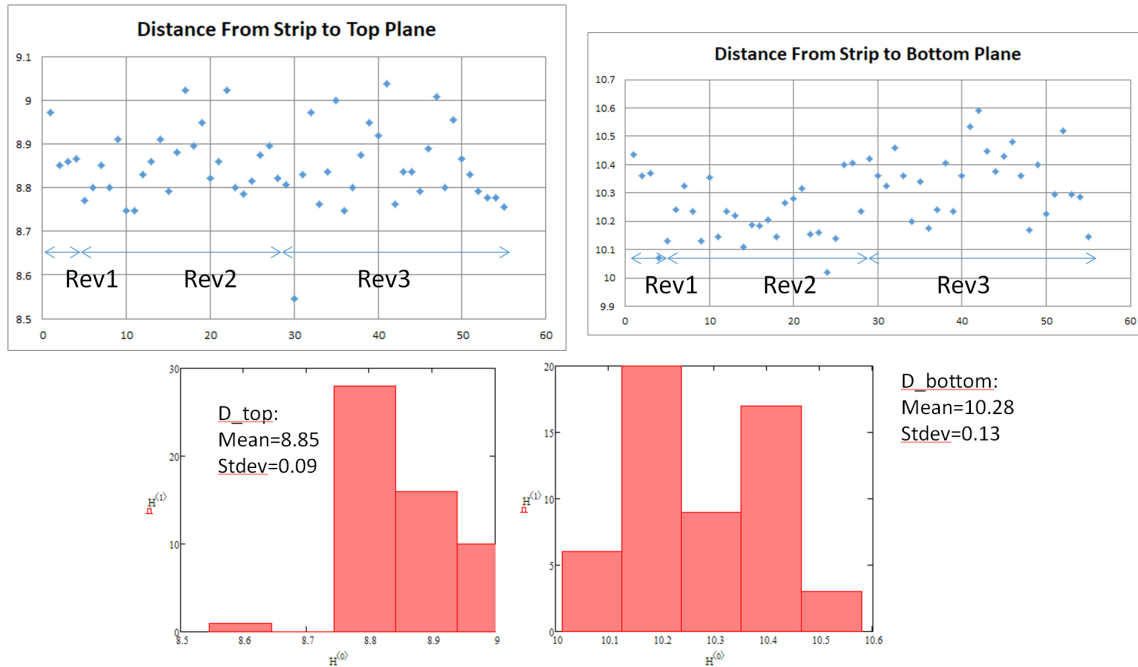


Fig. 7.3. Distance from top of the strip to the top metal plane (top left graph) and from the bottom of the strip to the bottom metal plane (top right graph) measured from cross-sections of all short strip line segments and corresponding histograms (bottom plots).

8. Dielectric and conductor loss separation

With the cross-sections geometry available, the material model parameters can be identified with high precision by matching measured and computed GMS-parameters or Gammas as outlined in section 3. The approach was tested in multiple projects like EvR-1 benchmark board [2], but never used for the ultra-low loss dielectrics and on the structures with the large variations of trace thickness as is in this case. The relative resistivity (RR) is the resistivity normalized to the bulk resistivity of annealed copper $1.724e-8 \text{ Ohm}\cdot\text{m}$. By following step 2 of the identification process outline in section 3, large variation of the identified relative resistivity is observed as illustrated in Fig. 8.1. RR was restricted by 1.8. The variations in the trace cross-section prevent accurate identification of the actual bulk resistivity of copper and the identified values are rather “effective resistivity”. Technically we have large variations in the trace cross-section of the traces that cannot be accounted in the resistivity identification and produce large variations of the effective resistivity. It also contributes to the uncertainty of the loss tangent identification (step 3 of the identification process from section 3).

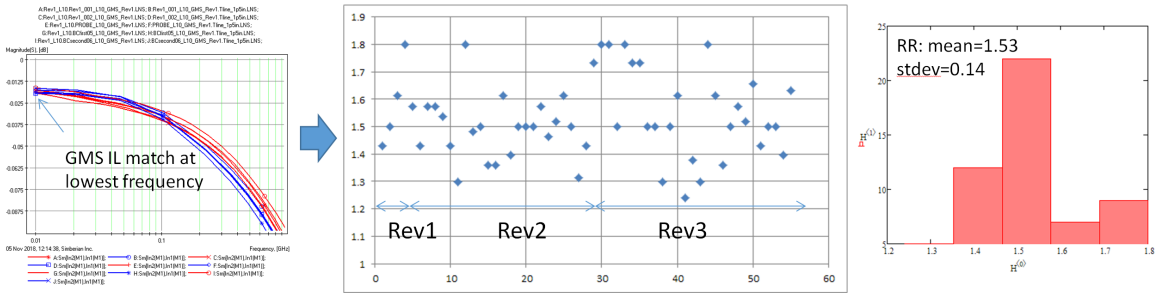


Fig. 8.1. Identification of the relative resistivity (RR) by matching GMS attenuation at the lowest frequency (illustrated on the left graph) produces large variations in RR.

According to the dielectric specifications from the manufacturer, the loss tangent should be 0.001 @ 1 GHz. The dielectric and conductor loss separation by matching loss tangent up to 2 GHz does not confirm this value if the identified value of the relative resistivity $RR=1.5$ is used as illustrated in Fig. 8.2. Either loss tangent should be even smaller than 0.001 @ 1 GHz (not likely), or the identified value of the resistivity should be smaller.

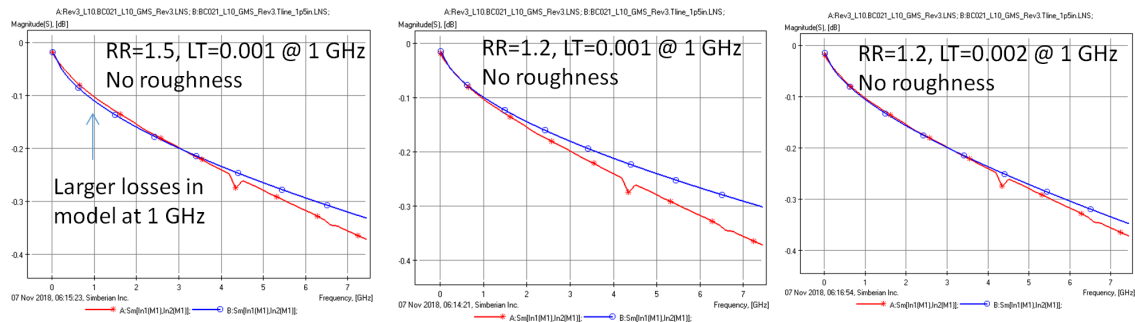


Fig. 8.2. Measured (red) and modeled GMS insertion loss. Identified value of the relative resistivity ($RR=1.5$) produces excessive losses (left plot) even with the minimal value of the loss tangent. Minimal value $RR=1.2$ provides more reasonable correlation of the insertion losses at lower frequencies (two right plots).

With the fixed value of $RR=1.2$ we can achieve very good correlation between measured and computed GMS insertion loss with both $LT=0.001$ and $LT=0.002$ as illustrated in Fig. 8.3. Fig. 8.4 and 8.5 further explain the problem with the loss separation. With the mean value of RR we will always have slightly excessive losses at lower frequencies if loss tangent values below 0.001 are not allowed. With $LT=0.001$ @ 1 GHz the dielectric losses are smaller than the conductor losses starting from about 3-4 GHz as shown in Fig. 8.4. The losses are comparable at lower frequencies and depend on both conductor cross-section and copper resistivity (or “effective resistivity” in our case). Most of the losses at higher frequencies come from the conductor and conductor roughness in this case. With larger value of the loss tangent $LT=0.002$, the dielectric losses are larger than the conductor but are still comparable as shown in Fig. 8.5 and sensitive to the effective resistivity. Considering this, we will try different variations of the identification algorithm with the fixed values of RR and LT and with simultaneous identification of RR and LT by matching GMS insertion loss at lower frequencies in the subsequent sections.

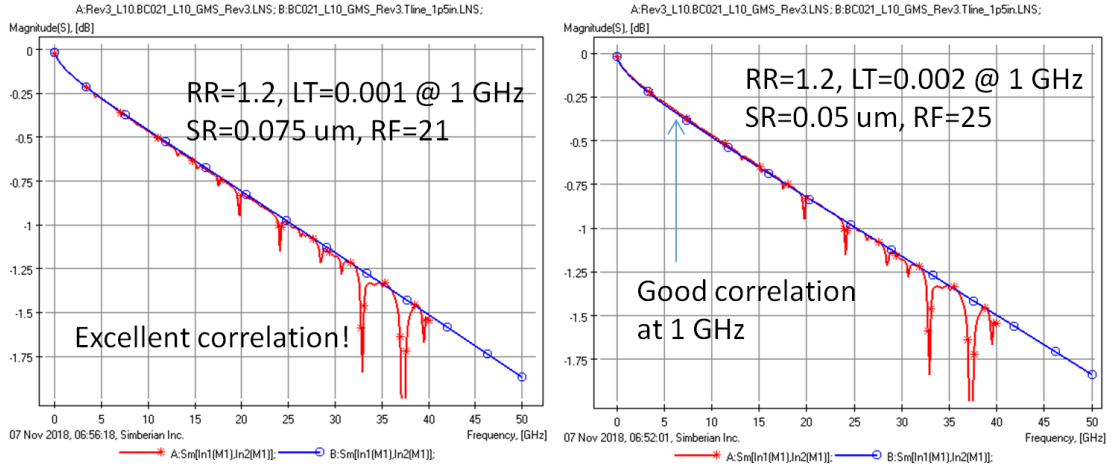


Fig. 8.3. Measured (red) and modeled GMS insertion loss for two possible outcomes of the material model identification with fixed loss tangent values. Losses are slightly larger at lower frequencies for the case of $LT=0.002$ @ 1 GHz

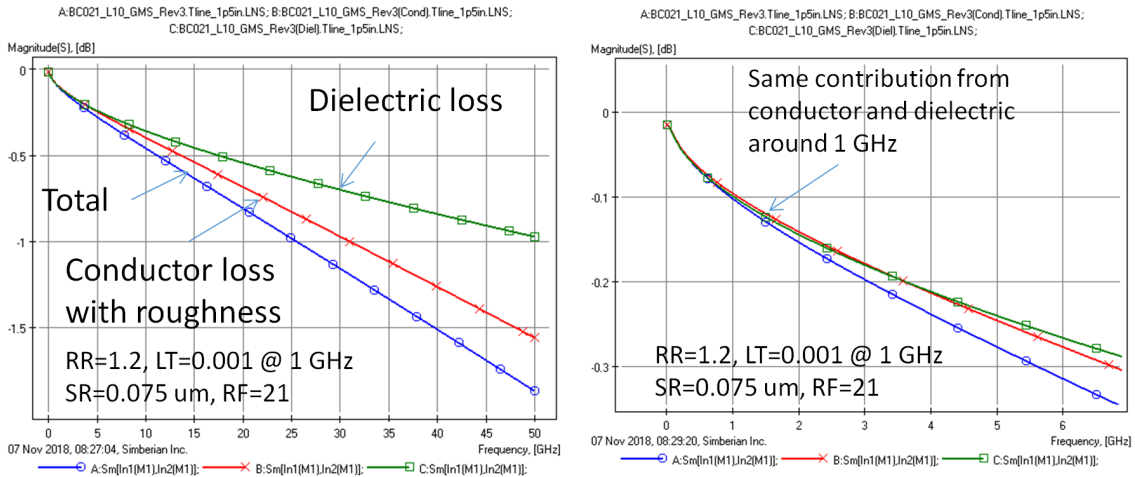


Fig. 8.4. Distribution of the losses between dielectric and conductor with $LT=0.001$ @ 1 GHz. Total losses match observed on one of the samples in Rev3.

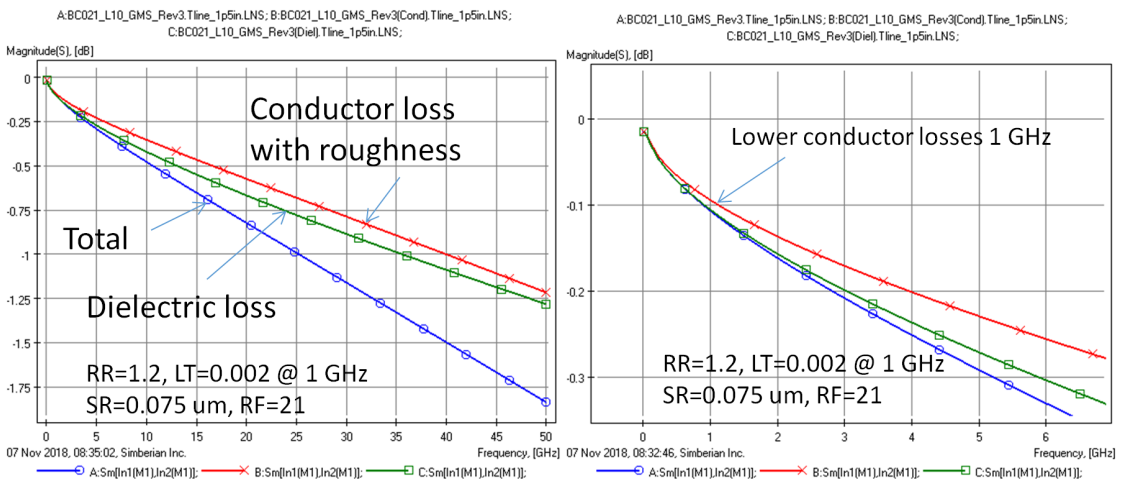


Fig. 8.5. Distribution of the losses between dielectric and conductor with $LT=0.002$ @ 1 GHz. Total losses match observed on one of the samples in Rev3.

9. Material model identification results

A few attempts of the material model identification were performed and just some cases that make sense are reported here. Direct use of the identification algorithm outlined in section 3 did not produce meaningful results because of the ultra-low loss dielectric and large variations in the strip cross-section and effective resistivity as explained in the previous section. The first modification of the algorithm was as follows:

- Cross-section geometry parameters as measured for the short line in each pair are used in the identification (assuming that the variations take place between the coupons only);
- Identify relative resistivity by matching GMS attenuation at 0.01 GHz with restriction of range from 1 to 1.8;
- Follow the original algorithm without the LT adjustment – fix $LT=0.001$ @ 1 GHz and identify Dk @ 1 GHz, then identify the roughness model parameters SR and RF, and finally correct Dk to match the phase delay;

Distributions of the identified conductor-related model parameters are shown in Fig. 9.1 and distributions of the dielectric constant are shown in Fig. 9.2 for all 55 samples in form of histograms (some outlier samples are removed). The vertical scale on all histograms is the number of cases in corresponding bin. Measurement to model correlation of GMS-parameters for Rev3 is shown in Fig. 9.3. As expected, the correlation of the attenuation at lower frequencies is not excellent – the model with the adjustment of resistivity overestimates the losses at lower frequencies (see explanation in the previous section). Though, the difference disappears at higher frequencies and we expect that this model will properly predict the attenuation up to 50 GHz and even at higher frequencies. Correlation for the phase delay is excellent and the model will work even above 50 GHz. Note that the strip cross-section in this case was also adjusted for each pair of strip segments with the data obtained for the short segment. The conductor loss model parameters are basically adjusted to have the attenuation observed from the measurements with changing cross-sections. This model is too complicated for the practical use and we proceed with some modifications of the model building process to simplify it and keep usable in the next section.

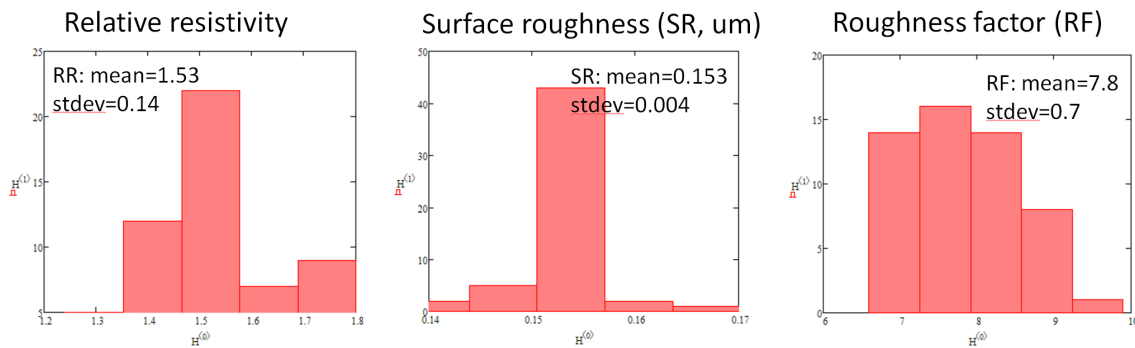


Fig. 9.1. Distribution of the identified conductor loss model parameters: relative resistivity (left) and two parameters of the Huray-Bracken roughness model (two right graphs).

Wideband Debye dielectric model – Dielectric constant (Dk @ 1 GHz)

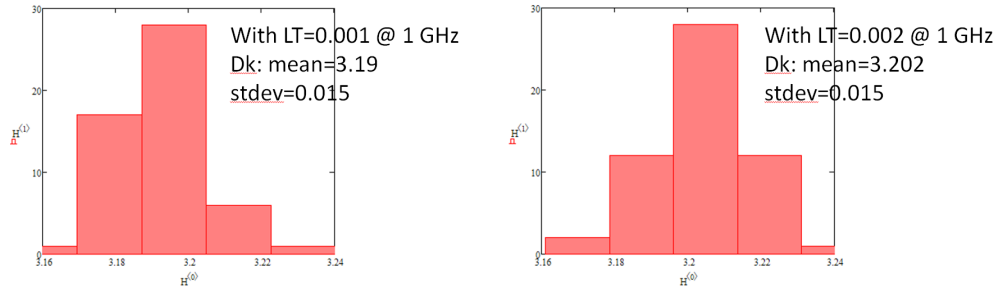


Fig. 9.2. Distribution of dielectric constant $Dk @ 1 \text{ GHz}$ for all 55 samples identified with fixed loss tangent values $LT=0.001$ (left) and $LT=0.002$ (right).

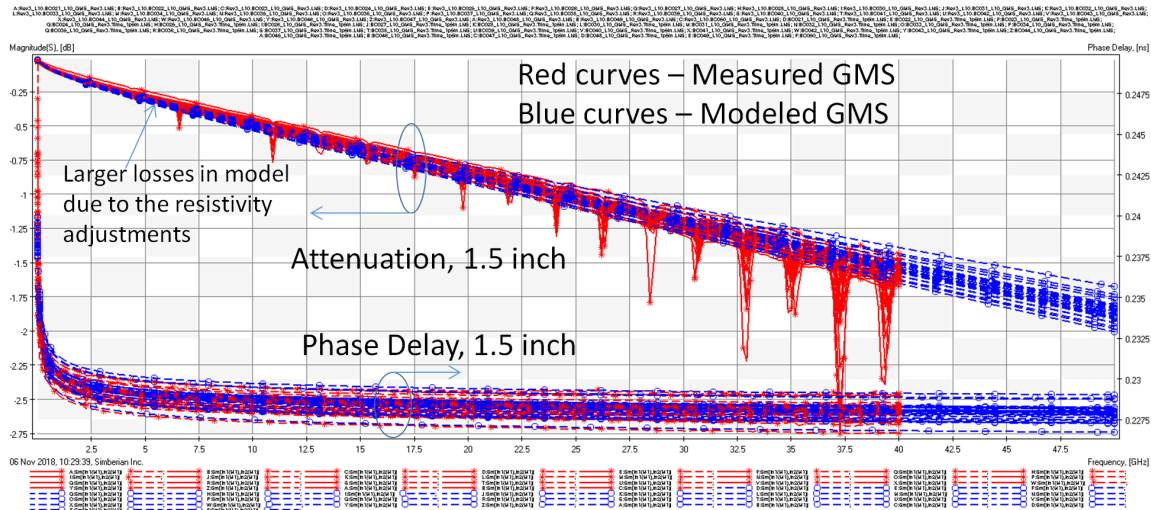


Fig. 9.3. Measured (red curves) and simulated (blue curves) GMS attenuation and phase delay for 28 cases from Rev3. Model parameters are identified with algorithm with fixed $LT=0.001 @ 1 \text{ GHz}$ and adjusted RR, Dk, SR and RF .

If we assume that the strip trace geometry variations are applicable not only to board to board variations, but also to each line segments (geometry changes along the segment), we can use the mean values of the geometry variations in the material model identification process and absorb all loss and delay variations into the material models. Here is the second modification of the identification process from section 3:

- Fix all cross-section parameters to mean values;
- Identify $Dk @ 1 \text{ GHz}$ first by matching GMS phase delay from 2 to 40 GHz
- Identify relative resistivity (RR) with loss tangent $LT @ 1 \text{ GHz}$ simultaneously by matching GMS attenuation from 0.01 to 2 GHz (restrict RR max value to 1.8);
- Identify roughness model parameters SR and by matching GMS attenuation from 2 to 25-35 GHz;
- Correct $Dk @ 1 \text{ GHz}$ by matching GMS phase delay from 2 to 40 GHz;

The results of this identification process for the batch Rev3 are shown in Fig. 9.4 for conductor models and in Fig. 9.5 for the dielectric model.

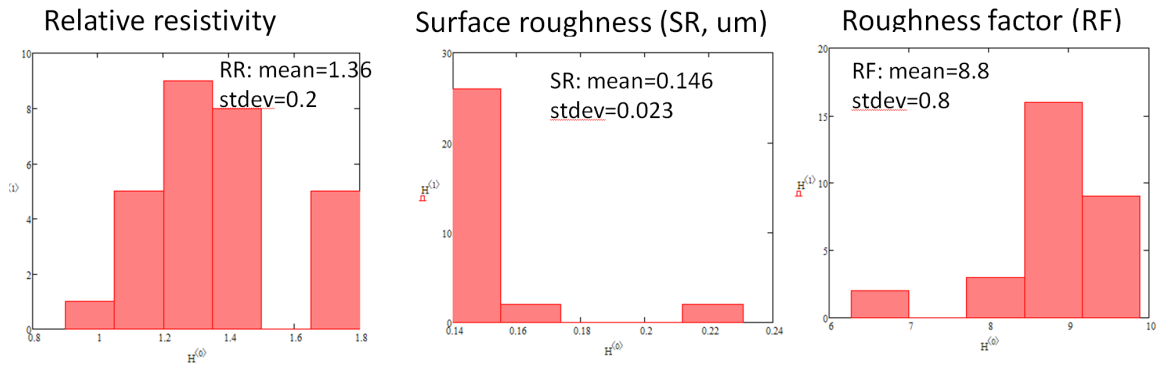


Fig. 9.4. Distribution of the identified conductor loss model parameters: relative resistivity (left) and two parameters of the Huray-Bracken roughness model (two right graphs) identified with algorithm with fixed cross-section geometry and with simultaneous identification of LT and RR and adjusted Dk, SR and RF.

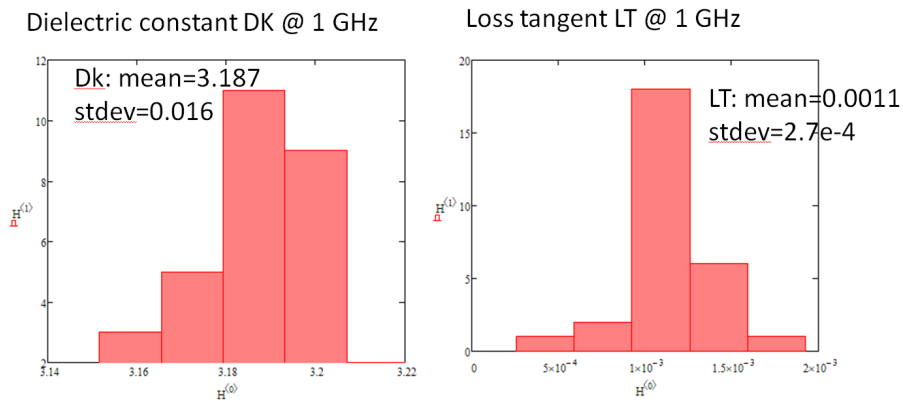


Fig. 9.5. Distribution of dielectric constant Dk @ 1 GHz (left) and loss tangent LT @ 1 GHz (right) identified with algorithm with fixed cross-section geometry and with simultaneous identification of LT and RR and adjusted Dk, SR and RF.

As we can see the mean value of the identified loss tangent is very close to the value from the manufacturer specifications. The identified mean value of the dielectric constant is about 3.19 – this is within the range from 3.12 to 3.23 provided by dielectric manufacturer and also within the range from 3.18 to 3.32 provided by the PCB manufacturer. Correlation of the model with the measured GMS-parameters is shown in Fig. 9.6. We can observe better correlation of the attenuation at the lower frequencies, but the variations of the losses observed in the experiment at lower frequencies are still larger than in reality. Variations of the transmission line characteristic impedance are evaluated for all 30 cases from Rev3 batch and is show in Fig. 9.7. The cross-section geometry is fixed in this case and all differences in the impedance are caused by the differences in the dielectric constant and in the roughness model (causal Huray-Bracken model changes the internal inductance of the strip that affects the delay as well as the characteristic impedance). The model predicts the mean value of the impedance 47.9 Ohm that correlates with the impedance observed on TDR for short line segment and about 1 Ohm lower than the impedance of the long line segments. Both impedances varies along the line segments about 1 Ohm – that variation is most likely due to dielectric constant change due to the fiber weave effect or variations of the conductor thickness. Overall, the second model can be considered acceptable. It is simpler than the first one, but is still way too complicated to be practical.

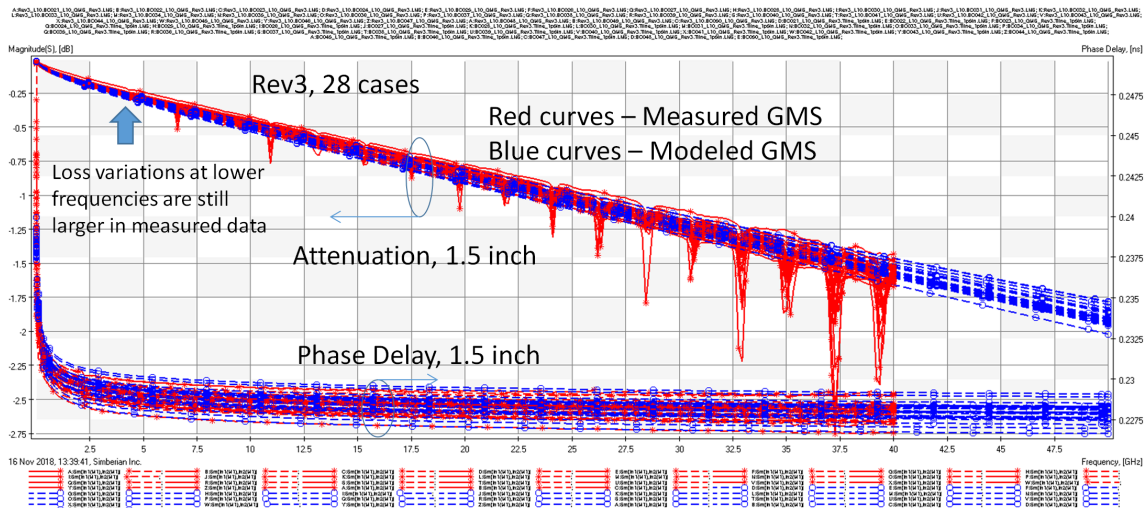


Fig. 9.6. Measured (red curves) and simulated (blue curves) GMS attenuation and phase delay for 28 cases from Rev3. Model parameters are identified with algorithm with the fixed cross-section geometry and simultaneous identification of LT and RR and adjusted Dk, SR and RF.

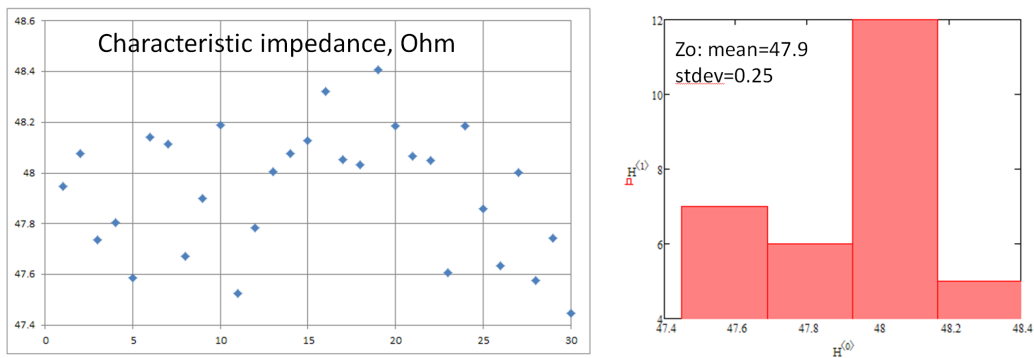


Fig. 9.7. Modeled impedance variations computed at 1 GHz with the model parameters identified with algorithm with fixed cross-section geometry and simultaneous identification of LT and RR and adjusted Dk, SR and RF.

10. Simplified models with statistical variables

To make a statistical model suitable for the practical analysis of 56 Gbps PAM4 links, we further simplified the material model identification algorithm from section 3 as follows:

- Fix all cross-section parameters to the mean values;
- Fix loss tangent LT @ 1 GHz to 0.001 or mean value 0.0011 identified earlier;
- Fix relative resistivity to mean value RR=1.5 identified earlier or to a “reasonable” value RR=1.2;
- Fix conductor roughness model parameter SR to either mean value identified earlier SR=0.15 μm or to some “reasonable” value;
- Identify roughness model parameter RF by matching GMS attenuation from 2 to 25-35 GHz;
- Identify Dk @ 1 GHz by matching GMS phase delay from 2 to 40 GHz;

This is the simplest procedure and the outcome is shown in Fig. 10.1. The simplified model correlates well with the measurements as shown in Fig. 10.2. All variations of the losses in this case are modeled with just one parameter – the roughness factor of the roughness correction coefficient (2.2)-(2.3).

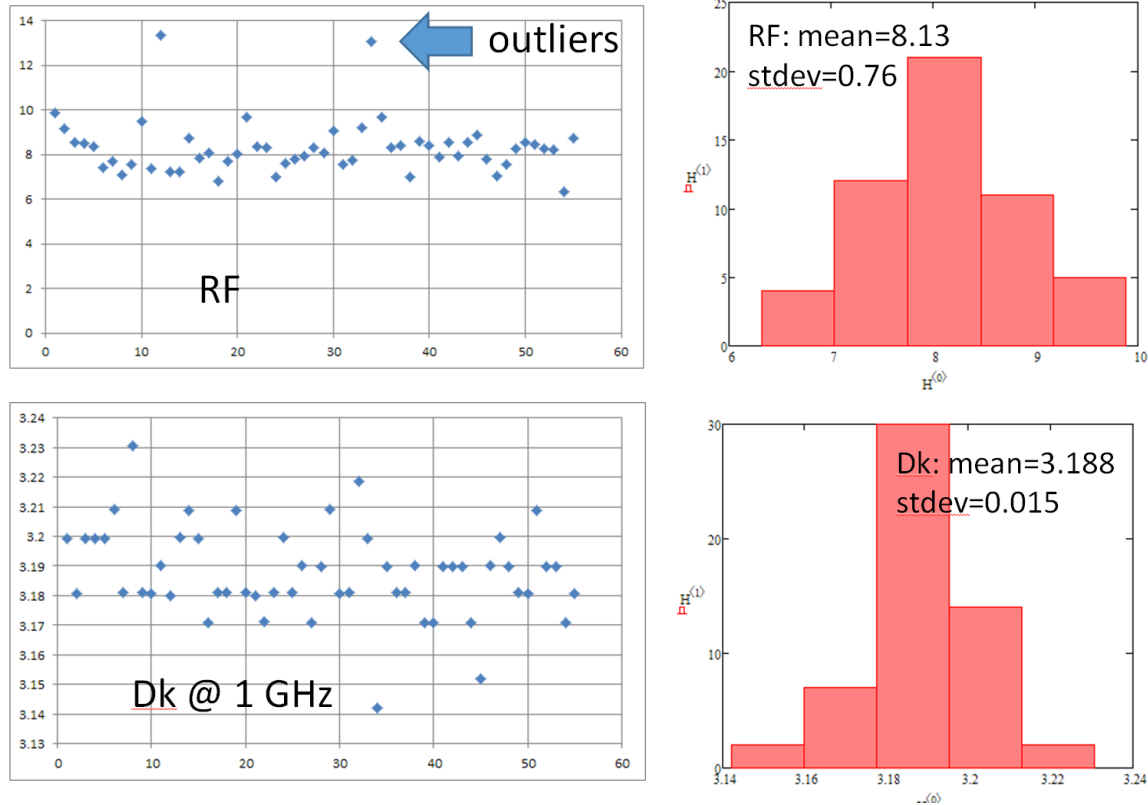


Fig. 10.1. Distribution of the roughness factor RF (top graph) and dielectric constant Dk @ 1 GHz (bottom graphs) identified with the fixed cross-section and $LT=0.001 @ 1 \text{ GHz}$, $SR=0.15 \text{ um}$, $RR=1.5$.

Most of the phase delay variations are modeled with the variations of the dielectric constant (the roughness contributes to phase delay variation too). Both variations of the Dk and RF contribute to the variations of the characteristic impedance – plots of the impedance for the limit cases are shown in Fig. 10.3. The model predicts about 1 Ohm difference between the limit cases. Note that the impedance is frequency-dependent and cannot be uniquely identified with the impedance values observed on TDR plots.

Finally, what can be done with the model parameters provided in Fig. 10.1. They can be used for the corner cases investigation. The distributions can be further converted into continuous distributions suitable for the statistical analysis of interconnects with the goal to define the yield. Note that the constructed model is very simple – just two variables that define the variations in the insertion loss, phase delay and characteristic impedance and correlate with the measurement. This is what we have achieved at this point of the project.

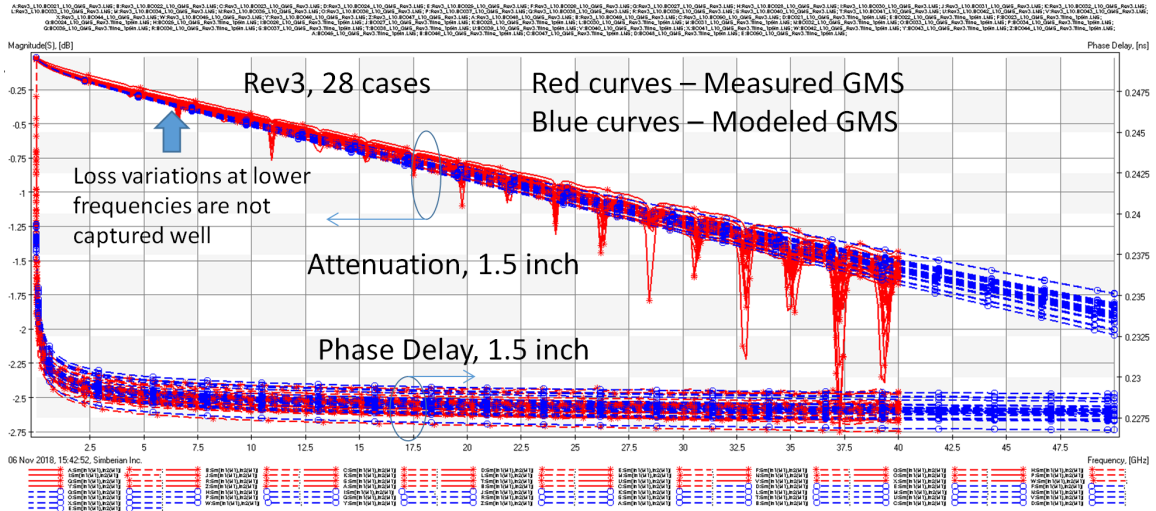


Fig. 10.2. Measured (red curves) and simulated (blue curves) GMS attenuation and phase delay for 28 cases from Rev3. Model parameters are identified with algorithm with the fixed cross-section geometry, $LT=0.001$ @ 1 GHz, $SR=0.15$ μm , $RR=1.5$ and adjusted RF and Dk.

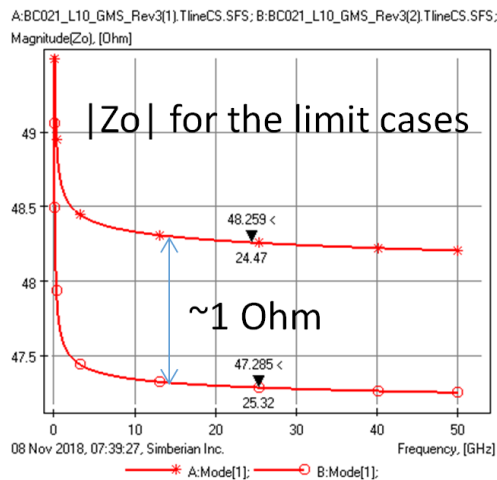


Fig. 10.3. Characteristic impedance limit cases with the model parameters identified with algorithm with fixed cross-section geometry, $LT=0.001$ @ 1 GHz, $SR=0.15$ μm , $RR=1.5$ and adjusted RF and Dk.

11. Conclusion

The results of the investigation reported here is the first step toward building simple statistical models for design of predictable interconnects for 56 Gbps PAM4 signals. We observed variations in the geometry and investigated multiple scenarios of the material model parameters identification with statistical variation. In the simplest model, variations in interconnect losses and dispersion are reduced to just two model variables with acceptable accuracy. The identified material models are practical and usable up to 50 GHz. It is observed that the trace geometry and roughness causes most of the loss variations in this ultra-low loss dielectric case. One of the surprises in the investigation is relatively small variations in identified dielectric constant. About half of the observed impedance variations can be attributed to the variations in dielectric constant and half to the conductor roughness. The rest is probably due to the geometry variations, such as

strip conductor thickness. Large observed variations in the strip conductor thicknesses was another surprise in this project. Note that this is project in progress. To add more certainty into the identification process, we plan to measure separately the bulk resistivity of copper. Also, we need to get rid of the peaks in the GMS insertion loss (they bias the results) by improving the test fixtures and GMS extraction algorithm. The final goal is to identify analytical distributions for the conductor and dielectric model parameters and may be for trace thickness and use them for compliance yield analysis of interconnects.

References

1. Y. Shlepnev, Moving from 28 Gbps NRZ to 56 Gbps PAM-4 - is it "free lunch"?, Design007 Magazine, August 2018 (available at <http://www.simberian.com/AppNotes.php>)
2. M. Marin, Y. Shlepnev, Systematic approach to PCB interconnects analysis to measurement validation, 2018 IEEE Symposium on Electromagnetic Compatibility, Signal and Power Integrity, July 30- August 3, 2018, Long Beach Convention Center, Long Beach, CA.
3. G. Brist, Design Optimization of Single Ended and Differential Impedance PCB Transmission Lines, 2004 - <https://www.jlab.org/eng/eecad/pdf/053designop.pdf>
4. C.Chia, R. Kunze, D. Boggs, M. Cromley, [A Study of PCB Insertion Loss Variation in Manufacturing Using a New Low Cost Metrology](#), IPC APEX EXPO, 2012
5. X. Ye, J. Hsu, K. Xiao, [Intel PCB Transmission Line Loss Characterization Metrology](#), Report to IPC D24D, 2017
6. R.M. Djordjevic, V.D. Biljic, Likar-Smiljanic, T.K. Sarkar, Wideband frequency domain characterization of FR-4 and time-domain causality, IEEE Trans. on EMC, vol. 43, N4, 2001, p. 662-667.
7. Y. Shlepnev, Unified approach to interconnect conductor surface roughness modelling, 2017 IEEE 26st Conference on Electrical Performance of Electronic Packaging and Systems (EPEPS2017), October 15-18, 2017, San Jose, CA..
8. Y. Shlepnev, Broadband material model identification with GMS-parameters, Proc. of 2015 IEEE 24st Conference on Electrical Performance of Electronic Packaging and Systems (EPEPS'2015), San Jose, 2015.
9. Y. Shlepnev, Y. Choi, C. Cheng, Y. Damgaci, Drawbacks and Possible Improvements of Short Pulse Propagation Technique, Proc. of 2016 IEEE 25st Conference on Electrical Performance of Electronic Packaging and Systems (EPEPS'2016), pp. 141-143, October 23-26, 2016, San Diego, CA.
10. Y. Shlepnev, A. Neves, T. Dagostino, S. McMorrow, Practical identification of dispersive dielectric models with generalized modal S-parameters for analysis of interconnects in 6-100 Gb/s applications, DesignCon 2010.
11. R. A. Soares, P. Gouzien, P. Legaud, G. Follot "A Unified mathematical approach to two-port calibration techniques and some applications", IEEE Trans. on MTT, v. 37, N 11 1989, pp. 1669-1674.
12. N. R. Franzen, R. A. Speciale, "A New Procedure for System Calibration and Error Removal in Automated S-Parameter Measurements", Proceedings of the 5th European Microwave Conference, Hamburg, Germany, 1-4 September 1975, pp. 69-73.